Vulnerability of Thalamic Nuclei at CSF Interface During the Entire Course of Multiple Sclerosis

Ismail Koubiyr, Takayuki Yamamoto, Simon Blyau, Reda A Kamroui, Boris Mansencal, Vincent Planche, Laurent Petit, Manojkumar Saranathan, Romain Casey, Aurélie Ruet, et al.

RESEARCH ARTICLE

Vulnerability of Thalamic Nuclei at CSF Interface During the Entire Course of Multiple Sclerosis

Ismail Koubiyr, PhD,* Takayuki Yamamoto, MD, PhD,* Simon Blyau, MD, Reda A. Kamroui, PhD, Boris Mansencal, MSc, Vincent Planche, MD, PhD, Laurent Petit, PhD, Manojkumar Saranathan, PhD, Romain Casey, MSc, Aurélie Ruet, MD, PhD, Bruno Brochet, MD, José V. Manjón, PhD, Vincent Dousset, MD, PhD, Pierrick Coupé, PhD, and Thomas Tourdias, MD, PhD, for OFSEP investigators

Correspondence
Dr. Koubiyr
ismail.koubiyr@u-bordeaux.fr

Neurol Neuroimmunol Neuroinflamm 2024;11:e200222. doi:10.1212/NXI.0000000000200222

Abstract

Background and Objectives

Thalamic atrophy can be used as a proxy for neurodegeneration in multiple sclerosis (MS). Some data point toward thalamic nuclei that could be affected more than others. However, the dynamic of their changes during MS evolution and the mechanisms driving their differential alterations are still uncertain.

Methods

We paired a large cohort of 1,123 patients with MS with the same number of healthy controls, all scanned with conventional 3D-T1 MRI. To highlight the main atrophic regions at the thalamic nuclei level, we validated a segmentation strategy consisting of deep learning–based synthesis of sequences, which were used for automatic multiatlas segmentation. Then, through a lifespan–based approach, we could model the dynamics of the 4 main thalamic nuclei groups.

Results

All analyses converged toward a higher rate of atrophy for the posterior and medial groups compared with the anterior and lateral groups. We also demonstrated that focal MS white matter lesions were associated with atrophy of groups of nuclei when specifically located within the associated thalamocortical projections. The volumes of the most affected posterior group, but also of the anterior group, were better associated with clinical disability than the volume of the whole thalamus.

Discussion

These findings point toward the thalamic nuclei adjacent to the third ventricle as more susceptible to neurodegeneration during the entire course of MS through potentiation of disconnection effects by regional factors. Because this information can be obtained even from standard T1-weighted MRI, this paves the way toward such an approach for future monitoring of patients with MS.

Introduction

Neuronal cell death, known as neurodegeneration, is the primary substrate of irreversible physical and cognitive disability in multiple sclerosis (MS).[1,2] In vivo, gray matter atrophy measured from MRI reflects neurodegeneration,[3] pointing toward such measurement as a relevant biomarker to monitor the patients under candidate therapies. In this perspective,

*These authors contributed equally to this work.

From the University of Bordeaux (I.K., T.Y., A.R., B.B., V.D., T.T.), INSERM, Neurocentre Magendie, U1215; Neuroimagerie diagnostique et thérapeutique (S.B.), CHU de Bordeaux; University of Bordeaux (R.A.K., B.M., P.C.), CNRS, Bordeaux INP, LABRI, UMR5800, Talence; Univ. Bordeaux (V.P.), CNRS, IMN, UMR 5293; Groupe d'Imagerie Neurofonctionnelle (L.P.), Institut des Maladies Neurodégénératives CNRS UMR 5293, Bordeaux, France; Department of Medical Imaging (M.S.), The University of Arizona, Tucson; Université de Lyon (R.C.), Université Claude Bernard Lyon 1, France; and Instituto de Aplicaciones de las Tecnologías de la Información y de las Comunicaciones Avanzadas (ITACA) (J.V.M.), Universitat Politècnica de València, Spain.

Go to Neurology.org/NN for full disclosures. Funding information is provided at the end of the article.

The Article Processing Charge was funded by the authors.

Glossary

BIC = Bayesian Information Criterion; **CIS** = clinically isolated syndrome; **CNN** = convolutional neural network; **EDSS** = Expanded Disability Status Scale; **HC** = healthy controls; **LME** = linear mixed effect; **MS** = multiple sclerosis; **PP** = primary-progressive; **RR** = relapsing-remitting; **SMD** = standardized mean difference; **SP** = secondary progressive; **WMn** = white-matter nulled.

highlighting the longitudinal profile of gray matter atrophy in time and space is highly desirable to monitor the effect of interventions on the relentless and progressive atrophic processes. However, currently, studies on the longitudinal evolution of gray matter atrophy are scarce[4] and inherently limited by a relatively short follow-up duration compared with the slow rate of atrophy progression.

In this context, the recent publications of brain charts for brain volumes derived from MRI over the entire lifespan provided a significant breakthrough,[5,6] where authors revealed the dynamic evolution of brain volumes from development to aging. Applying this framework—not only to global brain tissues but also to fine-grained structures—can open new perspectives to highlight the typical course of regions that can be particularly targeted in pathologic conditions. We have recently pioneered this approach to demonstrate an early divergence of specific amygdala-hippocampal and limbic structures in Alzheimer disease.[7-9]

Similarly, MS does not affect all gray matter regions equally.[10,11] Several pieces of evidence point toward the thalamus as a particularly vulnerable structure.[12,13] Its volume decreases from the earliest phases of MS,[14] with substantial clinical consequences.[15] White matter lesions are likely to transect fibers from the large fanning of the thalamocortical projections, inducing anterograde and retrograde degeneration,[16,17] which in turn contributes to such early thalamic atrophy.[13] More recently, the concept of differential vulnerability among thalamic nuclei also emerged[18] with histologic evidence of an "ependymal-in" gradient of thalamic damage related to meningeal inflammation affecting more particularly thalamic nuclei in contact with the third ventricle.[19] Therefore, certain groups of thalamic nuclei exposed to indirect (disconnection-related) but also to direct (meningeal inflammation-related) mechanisms might be affected earlier and more severely.

Along these lines, this study aimed at revealing the archetype dynamic volumetric profiles of thalamic nuclei groups during the course of MS. To do so, we took advantage of MRI data from more than a 1,000 patients with MS from a large multicenter cohort[20] that we paired with the same number of healthy controls from publicly available data sets. First, we investigated whether the whole thalamus was indeed the earliest and most severely affected brain structure in MS, using the recently developed brain chart approach.[8] Then, we tuned a deep learning–based algorithm that generated synthetic images from standard T1-weighted sequences available for all the participants, which allowed us to compute accurate volumes for thalamic nuclei groups. We concatenated all cross-sectional data of thalamic nuclei groups to infer their pseudolongitudinal course according to disease duration. We also investigated the possible underlying mechanisms and clinical performances associated with these dynamic patterns of thalamic nuclei atrophy.

Methods

Participants

This article is a secondary analysis based on the combination of prospectively collected cohorts. For MS, we leveraged a nationwide MS registry, initiated in 2011 and called OFSEP (Observatoire Français de la Sclérose en Plaques) that provided prospective and standardized data collection.[20] We extracted data from 2747 patients with MS included within the registry between 2011 and 2019 who fulfilled the following criteria: (1) a diagnosis of clinically isolated syndrome (CIS) or MS according to the 2010 McDonald Criteria[21] and (2) the presence of an MRI scan with at least 3D T1-weighted and T2-weighted/fluid-attenuated inversion recovery sequences. The Expanded Disability Status Scale (EDSS) and treatment status at the time of MRI examination were also requested. Disease duration was computed as the time between the MRI used in this analysis and the first clinical symptom suggestive of MS. A total of 2,413 healthy controls (HCs) were also included from open-access data sets (see eMethods).

To avoid age and gender bias, because these variables are directly related to the volumetry of brain structures,[7] the patients with MS were matched 1:1 to the HCs according to age ±1 year and sex using a greedy nearest neighbor matching algorithm without replacement. The pairing procedure led to the final inclusion of 1,123 participants perfectly matched in each group. Patients with MS included in the final analysis did not differ from the original population in disease severity [median (range) EDSS = 2 (0–9) vs median (range) EDSS = 2 (0–9), respectively; $p = 0.09$, standardized mean difference (SMD) = 0.09] and disease duration [mean (SD) disease duration = 11.49 (10.56) years vs mean (SD) disease duration = 10.65 (9.15) years, respectively; $p = 0.45$, SMD = 0.08].

Conventional T1 was the only available contrast for the volumetric analyses of these paired 1,123/1,123 patients with MS and HCs. We also took advantage of an additional group of 159 patients with MS explored with both conventional T1 and

Table 1 Descriptive Characteristics of the Participants

	Healthy controls (n = 1,123)	All MS (n = 1,123)	CIS (n = 236)	RRMS (n = 617)	SPMS (n = 171)	PPMS (n = 99)
Age, average ±SD	44.02 ± 15.68	44.01 ± 15.55	34.61 ± 13.73	41.60 ± 14.55	57.59 ± 8.79	57.89 ± 9.36
Sex (F/M)	634/489	634/489	122/114	368/249	103/68	41/58
Disease duration, average ±SD	—	11.50 ± 10.56	2.12 ± 3.68	11.62 ± 9.25	23.96 ± 9.61	11.53 ± 7.98
Median EDSS (Q1–Q3)	—	2.0 (1.0–4.0)	1.0 (0–1.5)	2.0 (1.0–3.5)	6.0 (4.5–6.5)	6.0 (4.0–6.5)
Median T2 lesion volume in ml (Q1–Q3)	—	6.36 (2.19–18.83)	2.34 (0.99–6.53)	6.18 (2.32–16.16)	20.35 (6.52–32.16)	11.44 (4.33–23.38)
Number of patients on DMTs (%)	—	644 (57.3%)	68 (28.8%)	444 (72%)	91 (53.2%)	41 (41.4%)

Abbreviations: CIS = clinically isolated syndrome; DMT = disease modifying treatment; EDSS = Expanded Disease Status Scale; MS = multiple sclerosis; PPMS = primary-progressive MS; RRMS = relapsing-remitting MS; SPMS = secondary-progressive MS.

white-matter nulled (WMn)-MPRAGE to be able to obtain synthetic WMn for all the participants (see eMethods).

Standard Protocol Approvals, Registrations, and Patient Consents

The OFSEP database was registered in ClinicalTrials.gov under the number NCT02889965. All patients gave consent to store their information in the database, which complies with French regulatory and General Data Protection Regulation requirements. The objectives and design of this secondary analysis were made publicly available on the website of the OFSEP (ofsep.org/en/studies).

MRI Data and Image Processing

MRI data from patients with MS were collected on scanners from different vendors, but they all followed recommendations and criteria of quality that were specified in the OFSEP centers.[22] Furthermore, all the images were preprocessed specifically to harmonize them as described elsewhere.[23] Then, all the preprocessed images underwent a stringent automatic quality control based on artificial intelligence. Finally, cortical and subcortical gray matter regions were segmented on the harmonized and quality-checked T1-weighted images using AssemblyNet, which combines 250 deep learning models through a multiscale framework.[23] We considered 124 gray matter structures in the following analyses according to the Neuromorphometrics labels.[24]

For patients with MS, the white matter T2-hyperintense lesions were also segmented using DeepLesionBrain.[25] The lesion masks were used to perform inpainting of MS lesions on T1-weighted images[26] to limit their impact on brain segmentation.

We trained a convolutional neural network (CNN) to generate synthetic WMn images from the conventional T1-weighted data following a variant of a previously published methodology[27] (see eMethods). After validating this approach, we used this deep learning algorithm on the T1-weighted images from the 1123 patients with MS and 1123 HCs to generate synthetic WMn, which, in turn, were used to segment the 4 main thalamic nuclei groups (anterior, medial, posterior, lateral) with the automated THOMAS algorithm.[28]

To understand the mechanisms associated with the atrophy of the thalamic nuclei groups, we estimated the impact of disconnection by MS white matter lesions. For that purpose, we reconstructed the thalamocortical bundles associated with each group of nuclei, computed the MS lesions falling "inside" or "outside" such bundles, and estimated the effect of each lesion category on the volume of the associated thalamic nuclei group (details are presented in eMethods).

Statistical Analyses and Model Generation

Continuous variables were expressed as means (SD) in the case of normal distribution or medians (interquartile range) otherwise. Categorical variables were expressed as numbers (percentage). The normality of distributions was assessed using histograms and Shapiro-Wilk test. Demographic characteristics were compared with Student t-test, Mann-Whitney test, or chi-square test as appropriate.

We first computed the volumetric trajectories of 124 gray matter structures according to disease duration by assembling the 1,123 cross-sectional data from the MS database to extrapolate a single longitudinal model. For that, we computed the Z-score for each structure using the mean and SD over the HC, allowing normalization and comparison between structures of different sizes. Then, as previously performed,[5,7,8] we tested various models to estimate the best trajectory of each structure from the simplest to the most complex (i.e., linear, quadratic, and cubic models). We kept a model as a potential candidate when F-statistic based on ANOVA (i.e., model vs constant model) was significant ($p < 0.05$), and all its coefficients were significant using t-statistic ($p < 0.05$). We used the Bayesian Information Criterion (BIC) to select the best candidate. This procedure was done for all the structures. The prediction bounds were estimated with a confidence level of 95%. A significant divergence between the trajectories of the patients and those of the HCs

Figure 1 Timeline of Gray Matter Structures Atrophy During the Course of MS

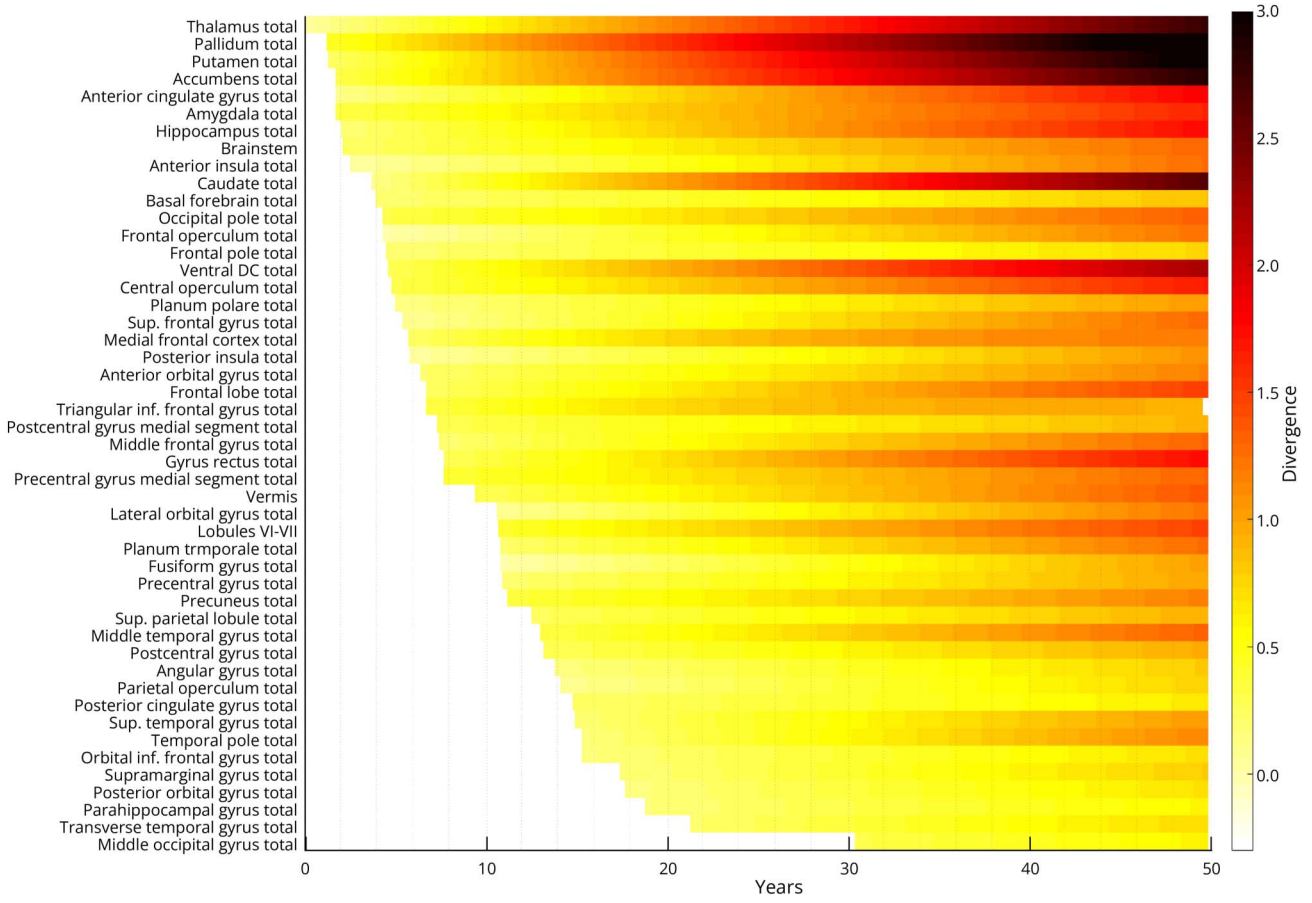

The color map represents the effect size of structural divergence compared with healthy controls along disease duration (DD).

was considered when the adjusted 95% CIs of the 2 models did not overlap. The sequence of divergence was listed in a chronological order.

Then, we moved to the thalamic nuclei group level. To validate the performance of THOMAS to compute the volumes of the thalamic nuclei from the synthetic WMn images, we compared dices and VSI using Student paired *t* test or Wilcoxon test when appropriate.

The volumetric Z-scores of the thalamic nuclei groups were calculated for the patients with MS as described above for the other gray matter structures. These Z-scores were first compared using linear mixed-effect (LME) models according to MS phenotypes (CIS, relapsing-remitting [RR], secondary progressive [SP], primary-progressive [PP]) and then according to quartiles of disease duration (<2.7, 2.7–8.4, 8.5–17, ≥18 years). In each LME model, we included the interaction between thalamic nuclei groups and the above-mentioned independent variables (phenotypes or disease duration), but also prespecified adjustment factors (age, sex, lesion load, and total intracranial volume) as fixed effects and subject as random effect (to take into account the repeated measures for each subject; 4 thalamic nuclei groups). Post hoc pairwise comparisons between each group were performed using linear contrast after applying a Bonferroni correction.

We also modeled the trajectories of the 4 thalamic nuclei groups continuously using the same method as described above for the other gray matter structures (concatenation of cross-sectional data into pseudolongitudinal models). A significant divergence between the trajectories of the different thalamic nuclei group was considered when the adjusted 95% CIs of 2 models did not overlap.

Then, we used another LME model to investigate the impact of T2 lesions "inside" tracts connected to specific thalamic nuclei and lesions "outside" of those tracts. For this, we included the volume of thalamic groups as the dependent variable, and we added the fixed effects of age, sex, disease duration, intracranial volume, and lesions "inside" and "outside" the specific thalamocortical bundles. Once again, participants were included as a random effect, and all variables were standardized to correctly compare estimates.

Finally, clinical associations between disease severity and thalamic nuclei groups were estimated with other LME models using EDSS as the dependent variable. Independent

Figure 2 Thalamic Nuclei Volumes per Phenotype and Disease Duration

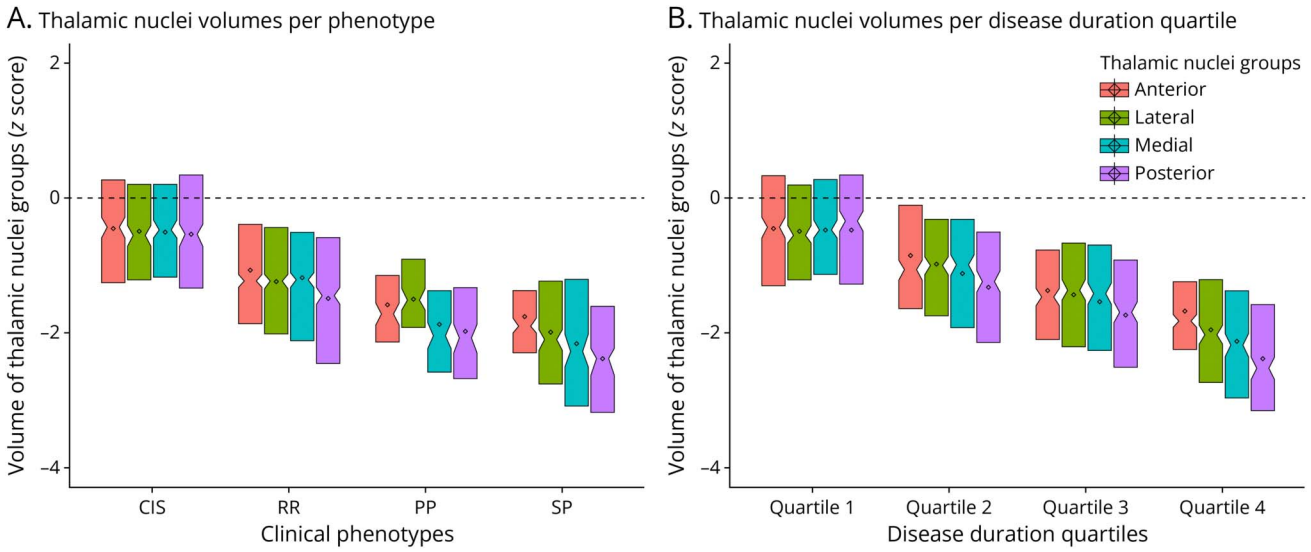

Volumes are represented as Z-scores with reference to the healthy control population. Thalamic volumes are displayed for each group of nuclei and for each clinical phenotype (A) and quartile of disease duration (B). Boxes represent median and interquartile range.

variables such as age, sex, lesion load, disease duration, whole thalamic volume, and the thalamic nuclei group were included as fixed factors if they were significant following a first univariate analysis. Significant LME models were then compared to find the one that best fits the data based on the likelihood ratio and the BIC. All continuous variables were also standardized to compare each impact.

Statistical testing was conducted at the two-tailed α-level of 0.05. Data were analyzed using the SAS software version 9.4 (SAS Institute, Cary, NC) and R (version 4.2.2).

Data Availability

The data that supported the findings of this study are available from the corresponding author upon reasonable request.

Results

Subject Characteristics

MRI data from 2,246 participants were analyzed, with 1,123 patients with MS corresponding to n = 236 CIS, n = 617 RR, n = 171 SP, and n = 99 PP patients. Table 1 summarizes the main characteristics of the participants. The patients with MS and HCs were perfectly matched over age and sex. All MS phenotypes had significantly different ($p < 0.001$) age (except SP vs PP), disease duration (except RR vs PP), EDSS (except SP vs PP), and lesion volume.

Timeline of Brain Structure Atrophy During the Course of Multiple Sclerosis

To start at the structure level, we first modeled the dynamic evolution of the gray matter structures segmented on T1-weighted images. Figure 1 illustrates the divergence between the patients with MS and the paired HC trajectories during the course of MS. The total volume of the thalamus was the first to become significantly smaller in patients with MS. Among the other gray matter structures to diverge early, we found the other deep gray nuclei, amygdala, and hippocampus but also highly connected regions such as the cingulate cortex, brainstem, or insula.

Thalamic Nuclei Volumes per Phenotypes and Disease Duration

To identify and analyze the main triggers of the earliest thalamic atrophy reported above, we moved at the substructure level, which corresponds to the thalamic nuclei. The first LME model explored the volumes of thalamic nuclei groups for the different clinical phenotypes and showed a significant effect of the clinical form ($p < 0.001$, $F = 25.38$) and nuclei group ($p < 0.001$, $F = 105.44$) with an interaction between both ($p < 0.001$, $F = 14.56$), independently from cofounders (age, sex, lesion load, and total intracranial volume). Overall, we found lower volumes from CIS to RRMS, PPMS, and then SPMS. We also found that the medial and posterior groups showed more severe atrophy (Figure 2A). Post hoc analysis showed that the 4 nuclei groups were comparable at the CIS stage (all $p > 0.05$). By contrast, they were all significantly different for patients with RRMS (all $p < 0.001$), with the posterior and medial showing the lowest volumes, followed by the lateral and anterior nuclei, respectively. Looking at the progressive forms, patients with PPMS showed significantly lower volumes for medial compared with anterior and lateral ($p < 0.001$), as well as for posterior compared with anterior and lateral ($p < 0.001$). At the same time, no difference was observed between medial and posterior and between anterior and lateral. Patients with SPMS showed a similar pattern,

Figure 3 Volume Trajectories of Thalamic Nuclei Groups in MS Over Disease Duration

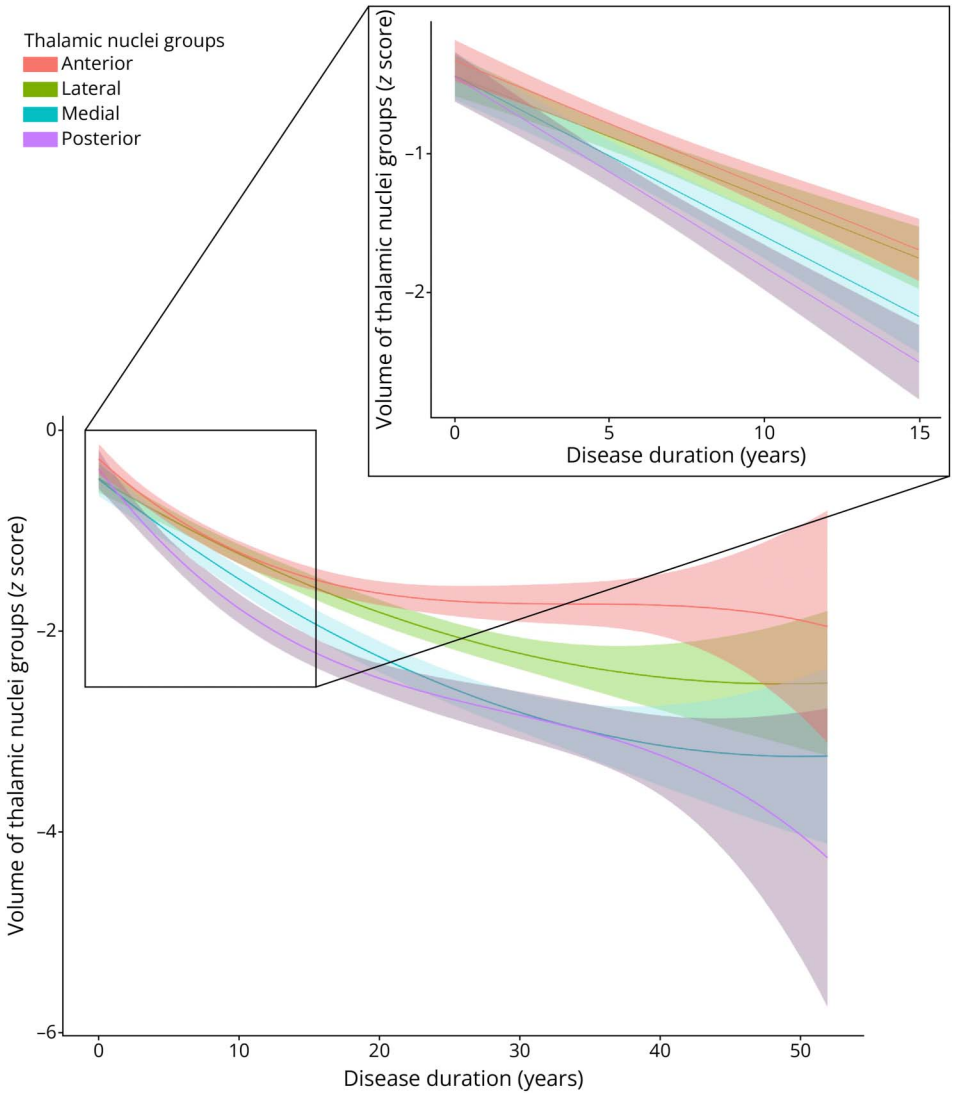

Volumes are represented as Z-scores with reference to the healthy control population. Strictly significant volumes differences were depicted when 2 CIs did not overlap anymore. Models that best fitted the data were selected for each nuclei group (see Statistical Analysis). The zoomed inset exhibits the trajectories during the 15 first years after disease onset, where a rapid divergence took place. During this shorter period, we could model the trajectories using a linear fitting to obtain the slopes (rates) of atrophy for each group.

except for a significantly lower volume of the lateral nucleus compared with the anterior one ($p < 0.001$).

A second LME tested the evolution of thalamic nuclei groups per disease duration. We also found a significant effect of the disease duration ($p < 0.001$, $F = 32.89$) and nuclei group ($p < 0.001$, $F = 149.64$) with an interaction between both ($p < 0.001$, $F = 21.58$). Figure 2B presents an earlier atrophy of posterior and medial groups compared with the lateral and anterior ones. The post hoc analysis showed comparable nuclei volumes for quartile 1 of disease duration. By contrast, quartile 2 already showed a significant difference between all nuclei volumes (all $p < 0.05$), with posterior and medial nuclei showing the most severe atrophy, followed by the lateral and anterior ones. As for quartile 3, the lowest volumes were observed with a similar pattern ($p < 0.05$), except for anterior and lateral regions, which were not significantly different ($p = 0.42$). Finally, larger atrophy was observed for quartile 4, again with a similar pattern to quartile 2 where all the nuclei were significantly different ($p < 0.05$), with larger atrophy in the medial and posterior regions.

Timeline of Thalamic Nuclei Volumes

To move to a continuous scale, while also considering the possibility of nonlinear evolutions, we managed to model the longitudinal trajectories of the 4 main thalamic nuclei groups through concatenation of all the cross-sectional data (Figure 3). We confirmed an earlier atrophy and divergence of the posterior group compared with both anterior and lateral groups (after a disease duration of 3 years and 4 years, respectively). Early volume loss was also noticed for the medial group showing differential atrophy compared with lateral and anterior nuclei after 8 years of disease duration. Lateral and anterior nuclei only showed significantly different volumes 24 years after disease onset, suggesting they have similar atrophy rates for a large range of the disease course.

Table 2 Linear Mixed-Effect Models for Thalamic Nuclei Volumes Association With Lesions Overlapping the Same Thalamocortical Projections

Nucleus	Age	Sex (M)	Duration	ICV	Lesions "inside"	Lesions "outside"
Anterior	−0.31[c]	−0.38[c]	−0.07[a]	0.17[c]	0.04	−0.38[c]
Lateral	−0.09[b]	−0.40[c]	−0.20[c]	0.56[c]	−0.34[c]	−0.28[c]
Medial	−0.14[c]	−0.38[c]	−0.25[c]	0.44[c]	−0.57[c]	−0.34[c]
Posterior	−0.19[c]	−0.21[b]	−0.26[c]	0.41[c]	−0.62[c]	−0.25[c]

Abbreviation: ICV = intracranial volume.
Values represent regression coefficients from the linear mixed model. All variables have been standardized (i.e., converted to Z-scores) for this analysis, and the coefficients are calculated for increase of 1 unit of Z-score of the independent variables.
[a] $p < 0.05$.
[b] $p < 0.01$.
[c] $p < 0.001$.

We looked more closely at the early evolution as it corresponded to the rapid divergence between groups. During the first 15 years of the disease course, volume trajectories were best modeled linearly with slopes representing the rate of atrophy (Figure 3, inset). We found steeper regression lines for both posterior and medial nuclei (−0.14 and −0.12, respectively) compared with the anterior and lateral ones (−0.08 and −0.08, respectively), indicating a faster rate of atrophy for these groups.

Relative Contributions of Primary and Secondary Mechanisms of Thalamic Nuclei Atrophy

To also estimate the contribution of disconnection-related atrophy, we quantified the impact of MS lesions on thalamic nuclei volumes when located specifically "inside" the thalamocortical projection of the given group (Table 2). To correctly compare the regression coefficient estimates, all variables have been previously standardized (i.e., converted to Z-score). We found that lesions "inside" contributed more than lesions "outside" for each group, expect the anterior one. This is probably related to the small size of the anterior nuclei group with fewer tracts connected to it.

We also observed that the same amount of demyelinating lesion overlap was associated with more atrophy when "inside" the projections of the posterior and medial groups (estimate [95% CI]: −0.62 [−0.69 to −0.54] and −0.57 [−0.66 to −0.48], respectively) than "inside" those of the lateral or anterior groups (estimate [95% CI]: −0.34 [−0.41 to −0.27] and 0.04 [−0.03 to 0.12], respectively).

This result suggests that atrophy induced by disconnection is potentiated in the medial and posterior groups.

Association Between Time Course of Thalamic Nuclei Atrophy and Disability

The first univariate correlations showed a significant association between EDSS and (1) age, (2) disease duration, (3) lesion load, (4) whole thalamus volume, and (5) the 4 nuclei groups. In multivariate analyses, 5 LME models were constructed (for the whole thalamus and each nuclei group, in addition to the previously reported significant covariates). This led to a significant model for the whole thalamus [estimate [95% CI] (*p*-value): −0.17 [−0.25 to −0.10] (<0.001)], as well as the anterior [−0.16 [−0.23 to −0.10] (<0.001)] and posterior group [−0.19 [−0.27 to −0.12] (<0.001)]. A final model combining these 2 previously significant nuclei groups showed a significant effect of age [0.31 [0.24–0.38] (<0.001)], disease duration [0.21 [0.13–0.28] (<0.001)], anterior group volume [−0.14 [−0.21 to −0.07] (<0.001)] and posterior group volume [estimate [−0.12 [−0.21 to −0.03] (<0.001)]. This last model (BIC = 1,515, loglikelihood = −730) was significantly better than the one with whole thalamic volume (BIC = 1,653, log-likelihood = −803). Details of these LME models are provided in the eTable.

Discussion

In this study, we highlighted the archetype dynamic evolution of intrathalamic atrophy during the course of MS. We revealed that medial and posterior groups of thalamic nuclei were exhibiting a faster atrophy rate than anterior and lateral groups. We argued for a "two-hit phenomenon" driving such a pattern; the effect of focal white matter lesions transecting thalamocortical projections being potentiated by other mechanisms affecting more particularly the medial and posterior groups which could be related to direct CSF-related inflammation.

Applying an innovative lifespan approach to a large MS cohort and matched healthy controls, we provided the first nonsupervised dynamic profile of regional volumes during a virtual course of 50 years of MS. We found regional variability in the trajectories of volume loss, with volume loss starting to affect deep gray matter nuclei, the amygdala/hippocampus complex, the brainstem, and, among the cortical ribbon, the insula and cingulum. The deep gray matter nuclei all showed up among the first structures to develop atrophy, the thalamus

being the first one, in line with thalamic atrophy that is already reported in pediatric MS,[29] relapse-onset MS,[30] CIS,[31] and radiologically isolated syndrome.[14] The cumulative effects of several mechanisms are likely responsible for the particular vulnerability of the deep nuclei.[13] The hippocampus and amygdala also showed early volume loss in our chart, which echoes the microstructural alterations reported from the CIS stage[32] attributed to the vulnerability of specific hippocampal synapses and spines to the strong microglial activation.[33] Brainstem vulnerability can be brought together with the observations of early spinal cord atrophy that is directly connected to the brainstem.[34] The insula and cingulum could be more vulnerable because they are also extensively connected and, therefore, more likely affected by remote effects of lesions along their connections. Postmortem data from longstanding MS donors have also reported the major alterations of insular and cingulate cortex at the contact of meningeal inflammation that was more abundant in the deep invagination of these structures.[10]

Altogether, the light shed on the thalamus with this novel approach strengthens the previous hypothesis-driven literature[12] and argues for deeper understanding at the substructure level, which requires investigating modification of the nuclei groups. However, in vivo parcellation of the thalamic nuclei through MRI is challenging. Here, we leveraged the strong intrathalamic contrast of a white matter–nulled version of T1 that we specifically tuned to maximize the internal thalamic contrast.[35] To enhance the real-world utility of this pulse sequence, currently not included in the standard protocol to monitor patients with MS,[36] we refined an MRI contrast synthesis strategy recently proposed to generate a synthetic WMn-MPRAGE.[27] Using the largest training database so far, with images from different vendors, we could train a robust CNN that can synthesize WMn images from standard T1 with specificity for MS because the training database was formed of patients with MS and not healthy controls as before.[27,37] We showed that this intermediate step was valuable to improve the accuracy of our automatic thalamic segmentation algorithm (THOMAS) that could then be used with WMn as an input as initially designed.[28] Overall, this approach is a breakthrough in terms of accuracy of intrathalamic segmentation, which was limiting the current nuclei analysis.

We reported a linear decrease of each thalamic nuclei group during the first 15 years of disease duration, which is consistent with a constant rate of atrophy already reported for the whole thalamus.[12] Of interest, the rates were different according to groups, with posterior and medial groups showing more rapid atrophy than anterior and lateral. These data extend the current literature that mainly consisted of cross-sectional data with too few patients to infer the timeline we could report here.[38-42] It is interesting to mention that It is interesting to mention that previous work showed that the thalamus shape was modified at the surface of the posterior and medial groups, and not at the surface of the lateral group in patients with MS.[39] In addition, while they used different segmentation approaches, the previous cross-sectional studies mainly reported a more particular vulnerability of the posterior group and relative sparing of the lateral group (also called ventral) at different stages.[38,40,41] Longitudinally, no difference in the rate of atrophy have been reported, likely because of the small sample size and short duration of follow-up.[39] The previous results on the anterior group are more conflicting[38,40,41] and should be taken into account with caution because of its small size and, therefore, prone to segmentation error. Accordingly, we found lower segmentation performance in dice score for the anterior group. Based on the comparison of the posterior, medial, and lateral groups, we concluded to a more substantial rate of atrophy for nuclei adjacent to the third ventricle, which could be the in vivo translation of the "ependymal-in" gradient reported pathologically[18,19] and associated to CSF-driven inflammation.[43] Such a differential rate of atrophy also echoes the microstructural gradient reported in pediatric MS,[44] and the subpial band-like thalamic lesions lining the ependymal surface of the third ventricle on 7T MRI.[45-47]

On top of such direct thalamic damages, white matter lesions can induce secondary thalamic degeneration, as argued for a long time.[16,17] To disentangle the effect of such an indirect mechanism from direct CSF-driven targeting, we rigorously quantified the effect of white matter lesions by quantifying their impact when specifically located inside or outside dedicated thalamocortical projections. We confirmed that lesions specifically located within thalamocortical projections affected the associated thalamic nuclei more than those outside. These results came from the comparisons of such a disconnection effect. We observed that the effect of the same volume of white matter lesion was more severe in thalamic nuclei atrophy when falling in the projections of the posterior or medial groups than in those of the lateral group. This observation argues again for additional factors within these groups (as discussed above) that potentiate the effect of disconnection. In inflammation, a cascade of events is implicated, one being able to potentiate the others, as shown with a two-hit model for the induction of an experimental MS-like lesion.[48] Our results argue that a regionally distributed factor (likely related to CSF) potentiates the effect of the widespread disconnection factor driving the spatial gradient of temporal trajectories reported here.

Thalamus volume has been correlated with clinical performances,[13,15] which can be related to its hub location at the center of several networks and its vulnerability to several mechanisms as discussed above. It is interesting that the whole thalamus volume could mix rapidly affected groups of nuclei and others that are more spared, which could dilute some effect. In line with this statement, we found that considering some groups could be more clinically relevant than considering the whole thalamus. The most clinically relevant groups of nuclei were those affected earlier (posterior group) and those that might have particular clinical implications (anterior group).[38,39]

Strengths of this study include (1) a large number of patients from a prospective, standardized, high-quality registry[20]; (2) an advanced imaging strategy to improve the accuracy of thalamic nuclei segmentation; and (3) careful consideration of the impact of white matter lesions according to their locations inside or outside specific thalamocortical projections. We also have to acknowledge limitations. Data from different scanners could have affected the results. However, the imaging protocol has been harmonized as much as possible across centers.[20] Furthermore, we preprocessed all the images centrally to improve homogeneity as already described.[8] Disease-modifying drugs may likewise affect the severity of atrophy, but could not be taken into account regarding the large panel of treatments in the cohort. A part of atrophy related to normal aging could corrupt the specific contribution of atrophy associated with MS. We limited such an aging effect by presenting all the results in Z-scores to measure the distance to a large control group perfectly matched for age and sex. Nevertheless, more than this might be needed to perfectly compensate the aging effect that could also be associated with some regional heterogeneity of volume loss.[49] While the thalamus is a cognitive hub,[50] we could not address the cognitive consequences of these differential trajectories as we had no standardized neuropsychological tests for those patients.

In conclusion, we report the archetype trajectories of regional volume loss in MS, which we modeled during more than 50 years of disease evolution. The results shed light not only on the earliest thalamus atrophy but also on its determinants. We argue for the heightening of neurodegeneration secondary to white matter lesions disconnecting the thalamocortical projections by regional factors associated with the CSF proximity of the third ventricle. Such 2 hits could explain the higher and almost consistent rate of atrophy for the medial and posterior groups of thalamic nuclei during MS evolution. These results pave the way toward understanding disease biology better, combining, for instance, these approaches with CSF profiling. It also opens perspectives to use such thalamic group volumetric methods as robust and relevant biomarkers in therapeutic trials and ultimately to monitor the disease course.

Acknowledgment

The NDAR data used in the preparation of this manuscript were obtained from the NIH-supported National Database for Autism Research (NDAR). This is supported by the National Institute of Child Health and Human Development, the National Institute on Drug Abuse, the National Institute of Mental Health, and the National Institute of Neurological Disorders and Stroke. A list of the participating sites and a complete list of the study investigators can be found at pediatricmri.nih.gov/nihpd/info/participating_centers.html. The ICBM data used in the preparation of this manuscript were supported by Human Brain Project grant PO1MHO52176-11 and Canadian Institutes of Health Research grant MOP-34996. The ABIDE data used in the preparation of this manuscript were supported by ABIDE funding resources listed at fcon_1000.projects.nitrc.org/indi/abide/. The ADNI data used in the preparation of this manuscript were obtained from the Alzheimer's Disease Neuroimaging Initiative (ADNI) (National Institutes of Health Grant U01 AG024904). The ADNI is funded by the National Institute on Aging and the National Institute of Biomedical Imaging and Bioengineering and through generous contributions from private partners as well as nonprofit partners listed at: ida.loni.usc.edu/collaboration/access/appLicense.jsp. Private sector contributions to the ADNI are facilitated by the Foundation for the National Institutes of Health (fnih.org). The grantee organization is the Northern California Institute for Research and Education, and the study was coordinated by the Alzheimer's Disease Cooperative Study at the University of California, San Diego. ADNI data are disseminated by the Laboratory for NeuroImaging at the University of California, Los Angeles. This research was also supported by NIH grants P30AG010129, K01 AG030514 and the Dana Foundation. The AIBL data used in the preparation of this manuscript were obtained from the AIBL study of ageing funded by the Commonwealth Scientific Industrial Research Organization (CSIRO; a publicly funded government research organization), Science Industry Endowment Fund, National Health and Medical Research Council of Australia (project grant 1011689), Alzheimer's Association, Alzheimer's Drug Discovery Foundation, and an anonymous foundation. See aibl.csiro.au for further details. Data used in the preparation of this article were also obtained from the Parkinson's Progression Markers Initiative (PPMI) database (ppmi-info.org). PPMI—a public-private partnership—was funded by The Michael J. Fox Foundation for Parkinson's Research and funding partners that can be found at ppmi-info.org/about-ppmi/who-we-are/study-sponsors. The OASIS data used in the preparation of this manuscript were obtained from the OASIS project funded by grants P50 AG05681, P01 AG03991, R01 AG021910, P50 MH071616, U24 RR021382, R01 MH56584. See oasis-brains.org/for more details. The authors thank all investigators of these projects who collected these datasets and made them freely accessible. This manuscript reflects the views of the authors and may not reflect the opinions or views of the database providers. The authors thank Maeva Kyheng and Julien Labreuche for support with statistical analyses.

Study Funding

This work benefited from the support of the project DeepvolBrain of the French National Research Agency (ANR-18-CE45-0013). This study was achieved within the context of the Laboratory of Excellence TRAIL ANR-10-LABX-57 for the BigDataBrain project. This study received financial support from the French government in the framework of the University of Bordeaux's France 2030 program/RRI "IMPACT". Moreover, the authors thank the French Ministry of Education and Research, and the CNRS for DeepMultiBrain project. This study has also been supported by the PID2020-118608RB-I00 grant from the Spanish Ministerio de Ciencia e Innovación.The MS data collection has been

supported by a grant provided by the French State and handled by the "Agence Nationale de la Recherche," within the framework of the "France 2030" programme, under the reference ANR- 10-COHO-002, Observatoire Français de la Sclérose en Plaques (OFSEP)" and "Eugène Devic EDMUS Foundation against multiple sclerosis".

Disclosure

The authors report no relevant disclosures. Go to Neurology.org/NN for full disclosures.

Publication History

Received by *Neurology: Neuroimmunology & Neuroinflammation* March 30, 2023. Accepted in final form January 19, 2024. Submitted and externally peer reviewed. The handling editor was Associate Editor Friedemann Paul, MD.

Appendix 1 Authors

Name	Location	Contribution
Ismail Koubiyr, PhD	University of Bordeaux, INSERM, Neurocentre Magendie, U1215, France	Drafting/revision of the manuscript for content, including medical writing for content; study concept or design; analysis or interpretation of data
Takayuki Yamamoto, MD, PhD	University of Bordeaux, INSERM, Neurocentre Magendie, U1215, France	Drafting/revision of the manuscript for content, including medical writing for content; analysis or interpretation of data
Simon Blyau, MD	Neuroimagerie diagnostique et thérapeutique, CHU de Bordeaux, France	Drafting/revision of the manuscript for content, including medical writing for content; analysis or interpretation of data
Reda A. Kamroui, PhD	University of Bordeaux, CNRS, Bordeaux INP, LABRI, UMR5800, Talence, France	Drafting/revision of the manuscript for content, including medical writing for content; analysis or interpretation of data
Boris Mansencal, MSc	University of Bordeaux, CNRS, Bordeaux INP, LABRI, UMR5800, Talence, France	Drafting/revision of the manuscript for content, including medical writing for content; analysis or interpretation of data
Vincent Planche, MD, PhD	Univ. Bordeaux, CNRS, IMN, UMR 5293, France	Drafting/revision of the manuscript for content, including medical writing for content
Laurent Petit, PhD	Groupe d'Imagerie Neurofonctionnelle, Institut des Maladies Neurodégénératives CNRS UMR 5293, Bordeaux, France	Drafting/revision of the manuscript for content, including medical writing for content; analysis or interpretation of data
Manojkumar Saranathan, PhD	Department of Medical Imaging, The University of Arizona, Tucson	Drafting/revision of the manuscript for content, including medical writing for content; analysis or interpretation of data
Romain Casey, MSc	Université de Lyon, Université Claude Bernard Lyon 1, F-France	Major role in the acquisition of data
Aurélie Ruet, MD, PhD	University of Bordeaux, INSERM, Neurocentre Magendie, U1215, France	Drafting/revision of the manuscript for content, including medical writing for content
Bruno Brochet, MD	University of Bordeaux, INSERM, Neurocentre Magendie, U1215, France	Drafting/revision of the manuscript for content, including medical writing for content
José V. Manjón, PhD	Instituto de Aplicaciones de las Tecnologías de la Información y de las Comunicaciones Avanzadas (ITACA), Universitat Politècnica de València, Spain	Drafting/revision of the manuscript for content, including medical writing for content; analysis or interpretation of data
Vincent Dousset, MD, PhD	University of Bordeaux, INSERM, Neurocentre Magendie, U1215, France	Drafting/revision of the manuscript for content, including medical writing for content
Pierrick Coupé, PhD	University of Bordeaux, CNRS, Bordeaux INP, LABRI, UMR5800, Talence, France	Drafting/revision of the manuscript for content, including medical writing for content; analysis or interpretation of data
Thomas Tourdias, MD, PhD	University of Bordeaux, INSERM, Neurocentre Magendie, U1215, France	Drafting/revision of the manuscript for content, including medical writing for content; study concept or design; analysis or interpretation of data

Appendix 2 Coinvestigators

Coinvestigators are listed at Neurology.org/NN.

References

1. Bjartmar C, Wujek JR, Trapp BD. Axonal loss in the pathology of MS: consequences for understanding the progressive phase of the disease. *J Neurol Sci.* 2003;206(2):165-171. doi:10.1016/s0022-510x(02)00069-2
2. Filippi M, Preziosa P, Copetti M, et al. Gray matter damage predicts the accumulation of disability 13 years later in ms. *Neurology*. 2013;81(20):1759-1767. doi:10.1212/01.wnl.0000435551.90824.d0
3. Filippi M, Bruck W, Chard D, et al.; Attendees of the Correlation between Pathological and MRI findings in MS workshop. Association between pathological and MRI findings in multiple sclerosis. *Lancet Neurol.* 2019;18(2):198-210. doi:10.1016/S1474-4422(18)30451-4
4. Eshaghi A, Marinescu RV, Young AL, et al. Progression of regional grey matter atrophy in multiple sclerosis. *Brain*. 2018;141(6):1665-1677. doi:10.1093/brain/awy088
5. Bethlehem RAI, Seidlitz J, White SR, et al. Brain charts for the human lifespan. *Nature*. 2022;604(7906):525-533. doi:10.1038/s41586-022-04554-y
6. Coupe P, Catheline G, Lanuza E, Manjon JV, Alzheimer's Disease Neuroimaging Initiative. Towards a unified analysis of brain maturation and aging across the entire lifespan: a MRI analysis. *Hum Brain Mapp.* 2017;38(11):5501-5518. doi:10.1002/hbm.23743
7. Coupe P, Manjon JV, Mansencal B, Tourdias T, Catheline G, Planche V. Hippocampal-amygdalo-ventricular atrophy score: Alzheimer disease detection using normative and pathological lifespan models. *Hum Brain Mapp.* 2022;43(10):3270-3282. doi:10.1002/hbm.25850
8. Planche V, Manjon JV, Mansencal B, et al. Structural progression of Alzheimer's disease over decades: the MRI staging scheme. *Brain Commun.* 2022;4(3):fcac109. doi:10.1093/braincomms/fcac109
9. Coupe P, Manjon JV, Lanuza E, Catheline G. Lifespan changes of the human brain in Alzheimer's disease. *Sci Rep.* 2019;9(1):3998. doi:10.1038/s41598-019-39809-8
10. Haider L, Zrzavy T, Hametner S, et al. The topography of demyelination and neurodegeneration in the multiple sclerosis brain. *Brain*. 2016;139(Pt 3):807-815. doi:10.1093/brain/awv398
11. Steenwijk MD, Geurts JJ, Daams M, et al. Cortical atrophy patterns in multiple sclerosis are non-random and clinically relevant. *Brain*. 2016;139(Pt 1):115-126. doi:10.1093/brain/awv337
12. Azevedo CJ, Cen SY, Khadka S, et al. Thalamic atrophy in multiple sclerosis: a magnetic resonance imaging marker of neurodegeneration throughout disease. *Ann Neurol.* 2018;83(2):223-234. doi:10.1002/ana.25150

13. Ontaneda D, Raza PC, Mahajan KR, et al.; North American Imaging in Multiple Sclerosis Cooperative NAIMS. Deep grey matter injury in multiple sclerosis: a naims consensus statement. *Brain*. 2021;144(7):1974-1984. doi:10.1093/brain/awab132
14. Azevedo CJ, Overton E, Khadka S, et al. Early CNS neurodegeneration in radiologically isolated syndrome. *Neurol Neuroimmunol Neuroinflamm*. 2015;2(3):e102. doi:10.1212/NXI.0000000000000102
15. Eshaghi A, Prados F, Brownlee WJ, et al.; MAGNIMS study group. Deep gray matter volume loss drives disability worsening in multiple sclerosis. *Ann Neurol*. 2018;83(2):210-222. doi:10.1002/ana.25145
16. Henry RG, Shieh M, Amirbekian B, Chung S, Okuda DT, Pelletier D. Connecting white matter injury and thalamic atrophy in clinically isolated syndromes. *J Neurol Sci*. 2009;282(1-2):61-66. doi:10.1016/j.jns.2009.02.379
17. Kolasinski J, Stagg CJ, Chance SA, et al. A combined post-mortem magnetic resonance imaging and quantitative histological study of multiple sclerosis pathology. *Brain*. 2012;135(Pt 10):2938-2951. doi:10.1093/brain/aws242
18. Pardini M, Brown JWL, Magliozzi R, Reynolds R, Chard DT. Surface-in pathology in multiple sclerosis: a new view on pathogenesis? *Brain*. 2021;144(6):1646-1654. doi:10.1093/brain/awab025
19. Magliozzi R, Fadda G, Brown RA, et al. "Ependymal-in" gradient of thalamic damage in progressive multiple sclerosis. *Ann Neurol*. 2022;92(4):670-685. doi:10.1002/ana.26448
20. Vukusic S, Casey R, Rollot F, et al. Observatoire francais de la sclerose en plaques (OFSEP): a unique multimodal nationwide MS registry in France. *Mult Scler*. 2020;26(1):118-122. doi:10.1177/1352458518815602
21. Polman CH, Reingold SC, Banwell B, et al. Diagnostic criteria for multiple sclerosis: 2010 revisions to the mcdonald criteria. *Ann Neurol*. 2011;69(2):292-302. doi:10.1002/ana.22366
22. Cotton F, Kremer S, Hannoun S, Vukusic S, Dousset V, Imaging Working Group of the Observatoire Français de la Sclérose en Plaques. OFSEP, a nationwide cohort of people with multiple sclerosis: consensus minimal MRI protocol. *J Neuroradiol*. 2015;42(3):133-140. doi:10.1016/j.neurad.2014.12.001
23. Coupe P, Mansencal B, Clement M, et al. Assemblynet: a large ensemble of CNNS for 3D whole brain MRI segmentation. *Neuroimage*. 2020;219:117026. doi:10.1016/j.neuroimage.2020.117026
24. Klein A, Tourville J. 101 labeled brain images and a consistent human cortical labeling protocol. *Front Neurosci*. 2012;6:171. doi:10.3389/fnins.2012.00171
25. Kamraoui RA, Ta VT, Tourdias T, Mansencal B, Manjon JV, Coup P. Deeplesion-brain: towards a broader deep-learning generalization for multiple sclerosis lesion segmentation. *Med Image Anal*. 2022;76:102312. doi:10.1016/j.media.2021.102312
26. Manjon JV, Romero E, Vivo-Hernando R, et al. Blind MRI brain lesion inpainting using deep learning. *International Workshop on Simulation and Synthesis in Medical Imaging*; 2020:41-49.
27. Umapathy L, Keerthivasan MB, Zahr NM, Bilgin A, Saranathan M. Convolutional neural network based frameworks for fast automatic segmentation of thalamic nuclei from native and synthesized contrast structural MRI. *Neuroinformatics*. 2022;20(3):651-664. doi:10.1007/s12021-021-09544-5
28. Su JH, Thomas FT, Kasoff WS, et al. Thalamus optimized multi atlas segmentation (thomas): fast, fully automated segmentation of thalamic nuclei from structural MRI. *Neuroimage*. 2019;194:272-282. doi:10.1016/j.neuroimage.2019.03.021
29. Mesaros S, Rocca MA, Absinta M, et al. Evidence of thalamic gray matter loss in pediatric multiple sclerosis. *Neurology*. 2008;70(13 Pt 2):1107-1112. doi:10.1212/01.wnl.0000291010.54692.85
30. Azevedo CJ, Cen SY, Jaberzadeh A, Zheng L, Hauser SL, Pelletier D. Contribution of normal aging to brain atrophy in MS. *Neurol Neuroimmunol Neuroinflamm*. 2019;6:e616. doi:10.1212/NXI.0000000000000616
31. Henry RG, Shieh M, Okuda DT, Evangelista A, Gorno-Tempini ML, Pelletier D. Regional grey matter atrophy in clinically isolated syndromes at presentation. *J Neurol Neurosurg Psychiatry*. 2008;79(11):1236-1244. doi:10.1136/jnnp.2007.134825
32. Planche V, Ruet A, Coupe P, et al. Hippocampal microstructural damage correlates with memory impairment in clinically isolated syndrome suggestive of multiple sclerosis. *Mult Scler*. 2017;23(9):1214-1224. doi:10.1177/1352458516675750
33. Bourel J, Planche V, Dubourdieu N, et al. Complement C3 mediates early hippocampal neurodegeneration and memory impairment in experimental multiple sclerosis. *Neurobiol Dis*. 2021;160:105533. doi:10.1016/j.nbd.2021.105533
34. Biberacher V, Boucard CC, Schmidt P, et al. Atrophy and structural variability of the upper cervical cord in early multiple sclerosis. *Mult Scler*. 2015;21(7):875-884. doi:10.1177/1352458514546514
35. Saranathan M, Tourdias T, Bayram E, Ghanouni P, Rutt BK. Optimization of white-matter-nulled magnetization prepared rapid gradient echo (MP-RAGE) imaging. *Magn Reson Med*. 2015;73(5):1786-1794. doi:10.1002/mrm.25298
36. Wattjes MP, Ciccarelli O, Reich DS, et al.; Magnetic Resonance Imaging in Multiple Sclerosis study group, Consortium of Multiple Sclerosis Centres, North American Imaging in Multiple Sclerosis Cooperative MRI guidelines working group. 2021 MAGNIMS-CMSC-NAIMS consensus recommendations on the use of MRI in patients with multiple sclerosis. *Lancet Neurol*. 2021;20(8):653-670. doi:10.1016/S1474-4422(21)00095-8
37. Manjon JV, Romero JE, Coupe P. Deep learning based MRI contrast synthesis using full volume prediction using full volume prediction. *Biomed Phys Eng Express*. 2021;8(1). doi:10.1088/2057-1976/ac3c64
38. Blyau S, Koubiyr I, Saranathan M, et al. Differential vulnerability of thalamic nuclei in multiple sclerosis. *Mult Scler*. 2023;29(2):295-300. doi:10.1177/13524585221114247
39. Bergsland N, Zivadinov R, Dwyer MG, Weinstock-Guttman B, Benedict RH. Localized atrophy of the thalamus and slowed cognitive processing speed in ms patients. *Mult Scler*. 2016;22(10):1327-1336. doi:10.1177/1352458515616204
40. Bergsland N, Benedict RHB, Dwyer MG, et al. Thalamic nuclei volumes and their relationships to neuroperformance in multiple sclerosis: a cross-sectional structural MRI study. *J Magn Reson Imaging*. 2021;53(3):731-739. doi:10.1002/jmri.27389
41. Levy S, Sandry J, Beck ES, Brandstadter R, Katz Sand I, Sumowski JF. Pattern of thalamic nuclei atrophy in early relapse-onset multiple sclerosis. *Mult Scler Relat Disord*. 2022;67:104083. doi:10.1016/j.msard.2022.104083
42. Bisecco A, Capuano R, Caiazzo G, et al. Regional changes in thalamic shape and volume are related to cognitive performance in multiple sclerosis. *Mult Scler*. 2021;27(1):134-138. doi:10.1177/1352458519892552
43. Bajrami A, Magliozzi R, Pisani AI, et al. Volume changes of thalamus, hippocampus and cerebellum are associated with specific csf profile in ms. *Mult Scler*. 2022;28(4):550-560. doi:10.1177/13524585211031786
44. De Meo E, Storelli L, Moiola L, et al. In vivo gradients of thalamic damage in paediatric multiple sclerosis: a window into pathology. *Brain*. 2021;144(1):186-197. doi:10.1093/brain/awaa379
45. Planche V, Su JH, Mournet S, et al. White-matter-nulled mprage at 7t reveals thalamic lesions and atrophy of specific thalamic nuclei in multiple sclerosis. *Mult Scler*. 2020;26(8):987-992. doi:10.1177/1352458519828297
46. Harrison DM, Oh J, Roy S, et al. Thalamic lesions in multiple sclerosis by 7T MRI: clinical implications and relationship to cortical pathology. *Mult Scler*. 2015;21(9):1139-1150. doi:10.1177/1352458514558134
47. Louapre C, Govindarajan ST, Gianni C, et al. Heterogeneous pathological processes account for thalamic degeneration in multiple sclerosis: insights from 7 T imaging. *Mult Scler*. 2018;24(11):1433-1444. doi:10.1177/1352458517726382
48. Kerschensteiner M, Bareyre FM, Buddeberg BS, et al. Remodeling of axonal connections contributes to recovery in an animal model of multiple sclerosis. *J Exp Med*. 2004;200(8):1027-1038. doi:10.1084/jem.20040452
49. Choi EY, Tian L, Su JH, et al. Thalamic nuclei atrophy at high and heterogenous rates during cognitively unimpaired human aging. *Neuroimage*. 2022;262:119584. doi:10.1016/j.neuroimage.2022.119584
50. Saalmann YB, Kastner S. The cognitive thalamus. *Front Syst Neurosci*. 2015;9:39. doi:10.3389/fnsys.2015.00039

Supplemental Material

eMethods

1. Population of healthy controls

To build a reference population across the entire lifespan for this analysis, we pooled a total of 2413 T1-weighted MRI of healthy controls (HC) from the following open-access datasets: NDAR (n=382, https://ndar.nih.gov), ABIDE (n=492, http://fcon_1000.projects.nitrc.org/indi/abide/), ICBM: (n=294 http://www.loni.usc.edu/ICBM/), IXI (n=549, http://brain-development.org/ixi-dataset/), ADNI1&2 (n=404, http://adni.loni.usc.edu), AIBL (n=232, http://www.aibl.csiro.au/), OASIS (n=298, https://www.oasis-brains.org), and PPMI (n=166, https://www.ppmi-info.org/).

2. Synthetic WMn-MPRAGE and thalamic nuclei segmentation: Methodology

On conventional T1-weighted images, the contrast between thalamic nuclei is poor, implicating that segmentation algorithms can, at best, infer the thalamic borders. A white matter-nulled (WMn) version of MPRAGE images drastically enhances the intra-thalamic contrast,[1] which is the rationale for the high performances of the original THOMAS (THalamus Optimized Multi Atlas Segmentation) algorithm.[2] To be able to use this original THOMAS algorithm, we trained a 3D convolutional neural network (CNN) specifically for MS application in order to generate synthetic WMn images from T1-weighted images, following a variant of a previously published methodology.[3] To train this MR contrast synthesis network, we used a database independent from the 1123 patients. It consisted of 159 pairs of WMn and T1 acquisitions (from different vendors) of MS patients collected as part of ongoing prospective studies (ClinicalTrials.gov no. NCT03692975, NCT01865357, NCT02290587, NCT03768648, NCT03455582, respectively). We divided these cases into a training set (80% of the data set *i.e.,* 127 pairs) and a test set (20% of the data set *i.e.,* 32 pairs).

To generate the synthetic WMn images we followed several steps. Specifically, we first increased the resolution of the preprocessed T1w images using an *in house* super-resolution algorithm based on a residual convolutional neural network architecture. This step, increased

the resolution from 1 mm^3 to 0.5 mm^3 resulting into a final volume size of 362x434x362 voxels. Then, the specifically trained CNN for MR image synthesis[4] was applied to the super-resolved images. Since the synthesis network was trained to generate MR volumes of size 181x217x181 voxels, this network was applied 8 times to the 8 strided versions (stride factor 2 in all 3 dimensions) of the super-resolved T1w images. Finally, the 8 generated synthetic WMn images were used to reconstruct the final ultra-high resolution WMn volume (362x434x362 voxels size) inverting the striding operation.

To test the relevance of this strategy, we used the test set (n=32) to run the THOMAS algorithm *(i)* on the native WMn but also *(ii)* on the synthetic WMn and *(iii)* the conventional T1. Considering THOMAS from native WMn as a gold standard, we quantified the quality of segmentations from the two other strategies in terms of dice score and volume similarity index (VSI). We summed the right and left sides together, and we gathered the 11 segmented nuclei in 4 main groups based on anatomical and functional considerations[5]: *(i)* the anterior group including the anteroventral nucleus, *(ii)* the lateral group including the ventral posterolateral, ventral lateral anterior, ventral lateral posterior and ventral anterior nuclei, *(iii)* the medial group including the mediodorsal and centromedian nuclei, and the habenula, and *(iv)* the posterior group including the pulvinar, medial geniculate and lateral geniculate nuclei.

3. Synthetic WMn-MPRAGE and thalamic nuclei segmentation: Validation

On T1-weighted images, the contrast between thalamic nuclei was poor (**eFig. 1A**) while it was enhanced on the WMn version (**eFig. 1B**) that is originally used in THOMAS segmentation algorithm.[2] The 3D CNN trained over 127 pairs of T1 and WMn acquisitions produced synthetic WMn images that were almost visually not distinguishable from the native ones (**eFig. 1C**).

On the 32 cases of the test set, we considered THOMAS segmentation from native WMn-MPRAGE to be the best case ("silver" standard) because we already validated this combination against histological ground truth.[1, 2] Compared to this reference, THOMAS applied to the synthetic WMn was significantly better than a variation of THOMAS applied directly to T1-weighted images[6] (**eFig. 1D**). For the thalamic nuclei groups, dice scores were improved from 0.64±0.10 to 0.88±0.02 ($p<0.001$) for the lowest values from the anterior group, and from 0.78±0.06 to 0.94±0.01 ($p<0.001$) for the highest values from the medial group. All the volume similarity indexes were also significantly improved when THOMAS was applied to synthetic

WMn rather than to T1-weighted images ($p<0.001$), with an important reduction of the standard deviations.

Overall, these results showed that using an intermediate step of WMn synthesis significantly improved the accuracy of thalamic nuclei segmentation when conventional T1 is the only available contrast.

4. Estimation of the effect of thalamo-cortical disconnection

To reconstruct the specific thalamocortical bundles for each thalamic nuclei group, we used diffusion-weighted and T1-weighted images of 20 healthy participants from the BIL&GIN database.[7] A whole-brain tractogram was built for each participant using the TractoFlow diffusion MRI processing pipeline.[8] The latter was made using the fiber orientation distribution function (fODF) image, inclusion and exclusion maps, ten seeds per voxel in the whole white matter mask, a step size of 0.5 mm, a maximum angle of 20°, and a streamline length between 10 and 250 mm. The 20 whole-brain tractograms were warped to the MNI space using ANTS.[9] We used ExTractorflow to filter out false-positive streamlines from each tractogram.[10] Then we performed the virtual dissection of the left and right thalamocortical bundles from these 20 anatomically-plausible whole-brain tractograms using the masks of the four thalamic nuclei groups in MNI[11] and regions of interest of the Johns Hopkins University template.[12] We used the stem/shell approach to extract only streamlines with one termination in the cortical grey matter but passing through a gyral stem and not crossing a gyral shell [Details in Figure 1 in [10]]. Four different thalamocortical bundles were composed of streamlines with the other termination in one of the specific thalamic nuclei groups in each hemisphere. A density map was computed for each left and right thalamocortical bundle from the 20 tractograms.

Finally, we quantified the overlap between these bundles and white matter lesions (lesions "inside" the projections) for each of our 1123 MS participants by multiplying the lesion load by the voxel weight (from 0.5 to 1.0) of the density map. The lesion volume "outside" the bundles was also quantified (**eFig. 2**).

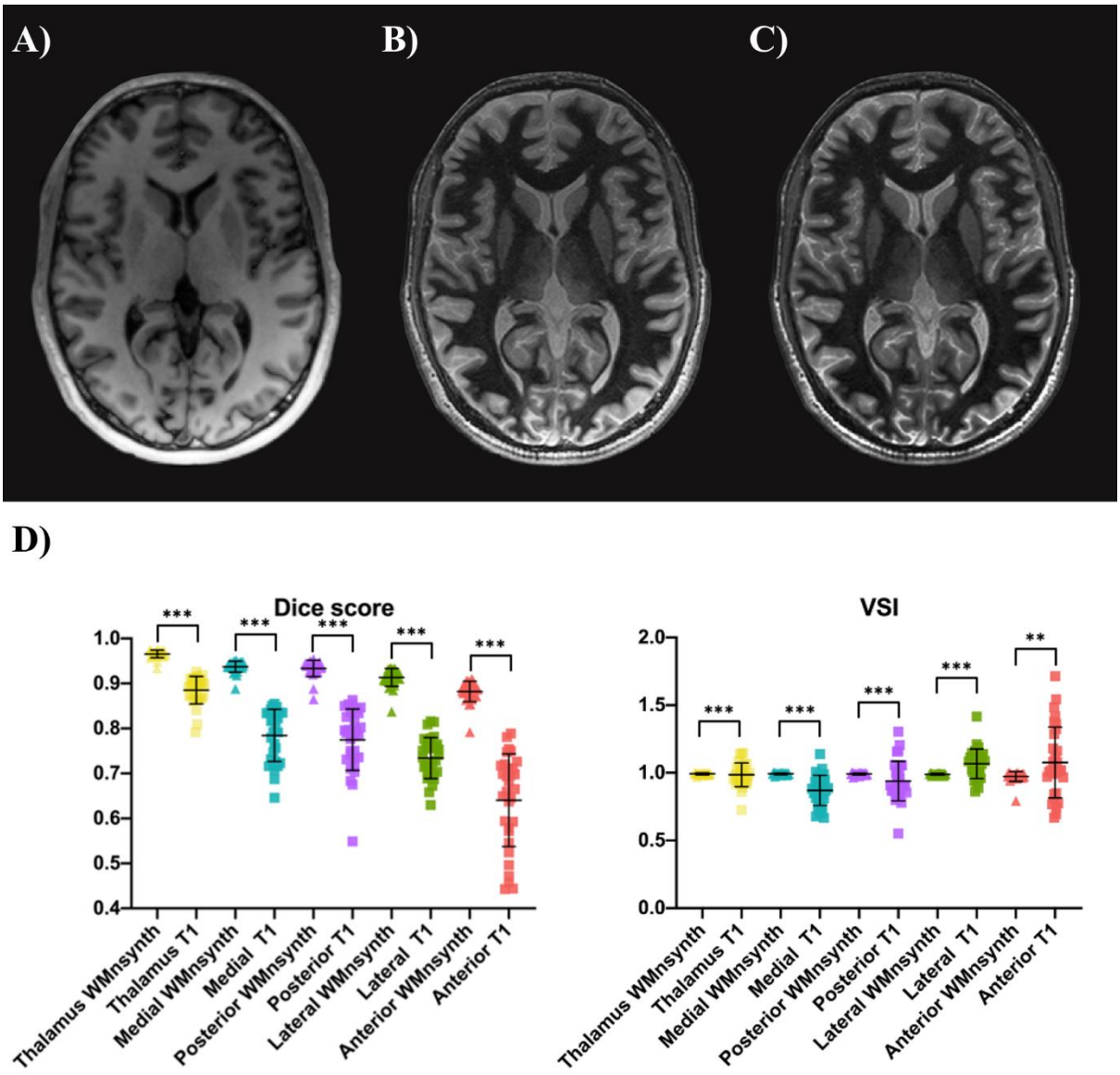

eFigure 1. Performance of synthetic WMn-MPRAGE for thalamic nuclei segmentation

Native T1-weighted image (A), native WMn-MPRAGE (B) and synthetic WMn-MPRAGE (C). Dices and volume similarity indexes (VSI) were computed when THOMAS was run on the native T1-weighted images or on the synthetic WMn-MPRAGE by comparison to the native WMn-MPRAGE used as the reference standard.

$^{*} < 0.05$; $^{**} < 0.01$; $^{***} < 0.001$.

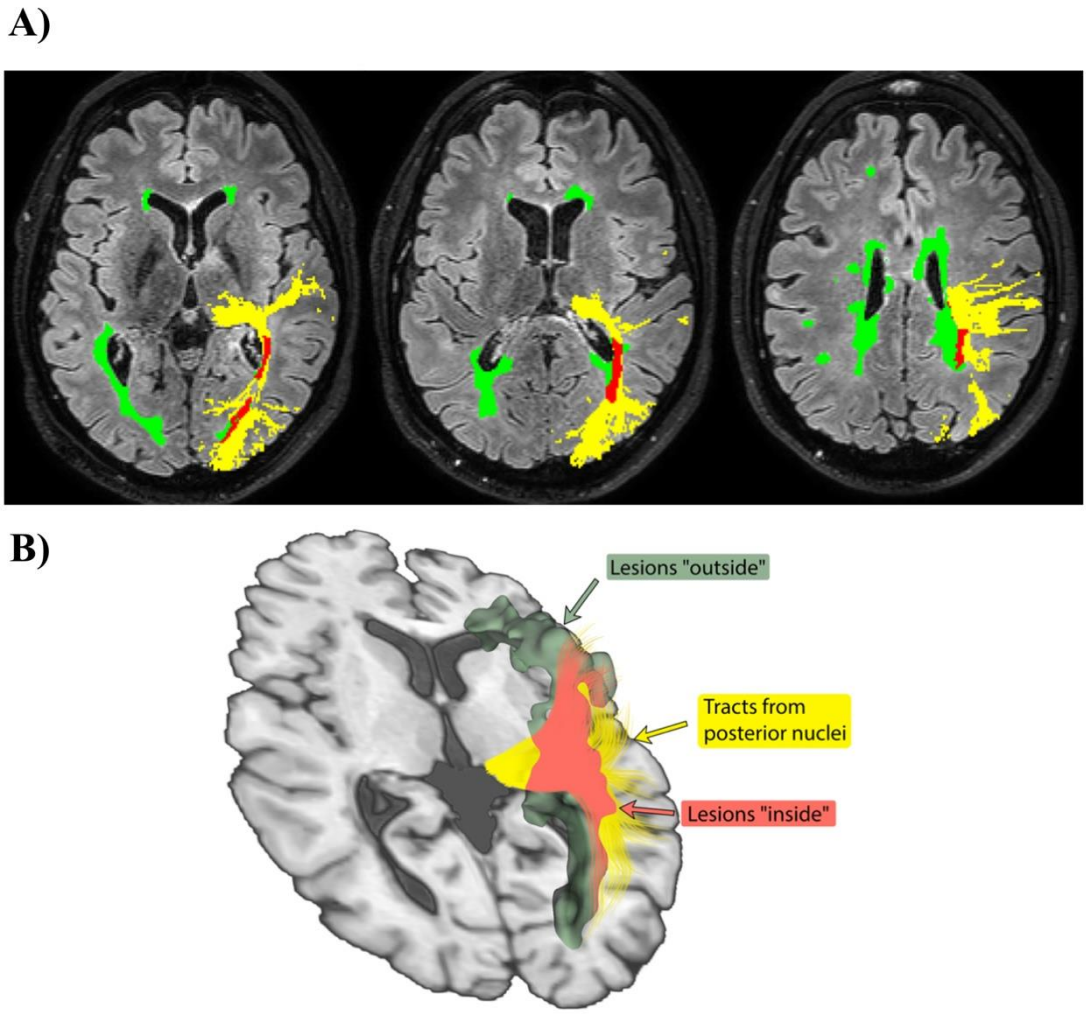

eFigure 2. Thalamo-cortical disconnection

Panel (A) displays tracts connected to the posterior thalamic group (in yellow), lesions overlapping these tracts (in red) and lesions outside these tracts (in green). Panel (B) represents a 3D visualization of the same the same subject.

eTable. Linear mixed effect models predicting disability (EDSS)

	Model		Predictor		
	BIC	**Loglikelihood**	**Estimate**	**CI**	**p**
Predicting EDSS with whole thalamus	**1653**	**-803**			
Age			0.35	0.28 – 0.42	**<0.001**
Disease duration			0.19	0.11 – 0.26	**<0.001**
Lesion load			0.05	-0.02 – 0.12	0.14
Whole thalamic volume			-0.17	-0.25 – -0.10	**<0.001**
Predicting EDSS with anterior nuclei	**1621**	**-787**			
Age			0.33	0.26 – 0.40	**<0.001**
Disease duration			0.22	0.15 – 0.29	**<0.001**
Lesion load			0.09	0.02 – 0.15	**0.009**
Anterior nuclei volume			-0.16	-0.23 – -0.10	**<0.001**
Predicting EDSS with lateral nuclei	**1530**	**-742**			
Age			0.35	0.28 – 0.42	0.15
Disease duration			0.23	0.16 – 0.30	0.21
Lesion load			0.11	0.04 – 0.17	0.30
Lateral nuclei volume			-0.09	-0.15 – -0.02	0.34
Predicting EDSS with medial nuclei	**1524**	**-738**			
Age			0.34	0.27 – 0.40	0.21
Disease duration			0.22	0.15 – 0.29	0.27
Lesion load			0.07	-0.00 – 0.13	0.46
Medial nuclei volume			-0.15	-0.22 – -0.08	0.33
Predicting EDSS with posterior nuclei	**1651**	**-802**			
Age			0.35	0.28 – 0.42	**<0.001**
Disease duration			0.18	0.11 – 0.26	**<0.001**
Lesion load			0.04	-0.03 – 0.11	0.22
Posterior nuclei volume			-0.19	-0.27 – -0.12	**<0.001**
Predicting EDSS with anterior and posterior nuclei	**1515**	**-730**			
Age			0.31	0.24 – 0.38	**<0.001**
Disease duration			0.21	0.13 – 0.28	**<0.001**
Lesion load			0.03	-0.04 – 0.10	0.38
Anterior nuclei volume			-0.14	-0.21 – -0.07	**<0.001**
Posterior nuclei volume			-0.12	-0.21 – -0.03	**0.007**

EDSS: expanded disability status scale; BIC: bayesian information criterion; CI: confidence interval.

eReferences

e1. Tourdias T, Saranathan M, Levesque IR, Su J, Rutt BK. Visualization of intra-thalamic nuclei with optimized white-matter-nulled mprage at 7t. *Neuroimage*. 2014;84:534-545

e2. Su JH, Thomas FT, Kasoff WS, Tourdias T, Choi EY, Rutt BK, et al. Thalamus optimized multi atlas segmentation (thomas): Fast, fully automated segmentation of thalamic nuclei from structural mri. *Neuroimage*. 2019;194:272-282

e3. Umapathy L, Keerthivasan MB, Zahr NM, Bilgin A, Saranathan M. Convolutional neural network based frameworks for fast automatic segmentation of thalamic nuclei from native and synthesized contrast structural mri. *Neuroinformatics*. 2022;20:651-664

e4. Manjon JV, Romero JE, Coupe P. Deep learning based mri contrast synthesis using full volume prediction using full volume prediction. *Biomed Phys Eng Express*. 2021;8

e5. Herrero MT, Barcia C, Navarro JM. Functional anatomy of thalamus and basal ganglia. *Childs Nerv Syst*. 2002;18:386-404

e6. Bernstein AS, Rapcsak SZ, Hornberger M, Saranathan M, Alzheimer's Disease Neuroimaging I. Structural changes in thalamic nuclei across prodromal and clinical alzheimer's disease. *J Alzheimers Dis*. 2021;82:361-371

e7. Mazoyer B, Mellet E, Perchey G, Zago L, Crivello F, Jobard G, et al. Bil&gin: A neuroimaging, cognitive, behavioral, and genetic database for the study of human brain lateralization. *Neuroimage*. 2016;124:1225-1231

e8. Theaud G, Houde JC, Bore A, Rheault F, Morency F, Descoteaux M. Tractoflow: A robust, efficient and reproducible diffusion mri pipeline leveraging nextflow & singularity. *Neuroimage*. 2020;218:116889

e9. Avants BB, Tustison NJ, Song G, Cook PA, Klein A, Gee JC. A reproducible evaluation of ants similarity metric performance in brain image registration. *Neuroimage*. 2011;54:2033-2044

e10. Petit L, Ali KM, Rheault F, Bore A, Cremona S, Corsini F, et al. The structural connectivity of the human angular gyrus as revealed by microdissection and diffusion tractography. *Brain Struct Funct*. 2022

e11. Saranathan M, Iglehart C, Monti M, Tourdias T, Rutt B. In vivo high-resolution structural mri-based atlas of human thalamic nuclei. *Sci Data*. 2021;8:275

e12. Oishi K, Faria A, Jiang H, Li X, Akhter K, Zhang J, et al. Atlas-based whole brain white matter analysis using large deformation diffeomorphic metric mapping: Application to normal elderly and alzheimer's disease participants. *Neuroimage*. 2009;46:486-499